Acta Materialia 132 (2017) 138–148

Contents lists available at ScienceDirect

Acta Materialia

journal homepage: www.elsevier.com/locate/actamat

Full length article

Ab initio modelling of solute segregation energies to a general grain boundary

Liam Huber [a, *], Blazej Grabowski [a], Matthias Militzer [b], Jörg Neugebauer [a], Jörg Rottler [c]

[a] Max-Planck-Institut für Eisenforschung GmbH, D-40237, Düsseldorf, Germany
[b] Centre for Metallurgical Process Engineering, The University of British Columbia, 309-6350 Stores Road, Vancouver, BC, V6T 1Z4, Canada
[c] Department of Physics and Astronomy, The University of British Columbia, 6224 Agricultural Rd., Vancouver, BC, V6T 1Z1, Canada

ARTICLE INFO

Article history:
Received 23 January 2017
Received in revised form
11 April 2017
Accepted 11 April 2017
Available online 18 April 2017

Keywords:
Ab initio modelling
Multiscale modelling
Grain boundary
Solute segregation

ABSTRACT

We apply a quantum mechanical/molecular mechanical (QM/MM) multiscale approach to calculate the segregation energies of Mg and Pb to two kinds of grain boundaries in Al. The first boundary, a symmetric (310)[001] Σ5 tilt boundary, is also tractable using traditional QM calculations, and serves as a validation for the QM/MM method. The second boundary is a general, low-symmetry tilt boundary that is completely inaccessible to pure QM calculations. QM/MM results for both of these boundaries are used to evaluate the accuracy of empirical (EAM) potentials for the Al-Mg and Al-Pb alloy systems. Based on these results we develop a physical model for the segregation energy based on elastic interaction and bond breaking terms. Both MM calculations with the EAM potentials and the model work quantitatively well for describing Mg-GB interaction across a wide range of local environments. For Pb, MM performance is weaker and the model provides only qualitative insight, demonstrating the utility of a QM/MM approach.

1. Introduction

From Hall-Petch strengthening to crack formation, grain boundary (GB) evolution plays a critical role in determining macroscopic material properties. In alloyed materials, GBs often serve as sinks for solute particles due to attractive GB-solute interactions. Because of this, even relatively small concentrations of alloying elements can have a significant impact through effects such as solute-drag reducing GB mobility, or GB embrittlement. Quantum mechanical (QM) density functional theory (DFT) calculations are a powerful tool for studying this interaction in great detail. Unfortunately, because of the high computational cost of DFT, such calculations are restricted to a small number of atoms—$\mathcal{O}(100)$. Because of this, QM calculations of GBs can typically be performed only on the small number of high-symmetry coincident site lattice (CSL) boundaries, whose structure repeats over short enough distances to fit within the periodic boundary conditions (BCs) that are applied in DFT calculations of metals. Results from such calculations are then taken as representative of a much broader class of general, low symmetry GBs, although the local atomic environment may differ substantially. Further, even for boundaries which are tractable in DFT, it is often difficult to obtain results which are well converged with respect to supercell size [1], i.e. which adequately control for long range solute-solute interaction between periodic images.

By contrast, classical molecular mechanical (MM) calculations which rely on empirical potentials are much more computationally efficient and can easily simulate very large structures with $\mathcal{O}(10^6)$ atoms, allowing for very complex GB structures. However, while MM simulations are comparatively inexpensive to perform, the development of a state-of-the-art embedded atom method (EAM) potential to represent host-host, host-solute, and solute-solute interactions represents significant overhead. This is compounded by the fact that new potentials must be generated for each set of alloying elements, which inhibits the study of chemical trends in solute behaviour across parts of the periodic table, as can commonly be found in DFT literature. Lastly, the accuracy of such potentials is constrained by the data with which they are constructed, so there is no guarantee that they will perform accurately for a given GB.

One approach is to combine the strengths of each of these techniques using QM/MM multiscale methods, in which a small region of interest (e.g. a solute atom and its neighbourhood) is

* Corresponding author.
E-mail address: huber@mpie.de (L. Huber).

http://dx.doi.org/10.1016/j.actamat.2017.04.024

represented using QM, and this is embedded in a much larger MM domain [2,3]. In this way, locally important electronic effects are captured in the small QM region, while long range elastic interactions are accounted for in the much larger MM domain. Here, we utilize recent improvements in QM/MM methodology [4] to treat Mg- and Pb-segregation to two GBs in Al. Mg is a common alloying element for Al and of great technological significance. Pb, while not as common in Al-based alloys, has a much larger size misfit relative to Al and a more complex electronic structure than Mg leading to longer ranged interactions [5], making it a good solute for testing the capabilities of the QM/MM technique.

The first boundary we study is the symmetric (310)[001] Σ5 tilt boundary, which has three unique GB sites. Because this boundary can also be studied with conventional QM methods, we use this system to demonstrate the accuracy of the QM/MM method when compared to DFT results. The second boundary is a general, low-symmetry tilt boundary, which is inaccessible by standard DFT. Here we select four sites to study using QM/MM. We also calculate segregation energies to all seven sites at both GBs using regular MM calculations with the EAM potentials of Mendelev et al. [6] and Landa et al. [7] for Al-Mg and Al-Pb, respectively. We then evaluate the performance of these potentials by comparison to QM/MM results. We finally study a much larger number of sites on the general boundary with MM only.

Atomistic methods can yield quantitative results, but it can sometimes be opaque *why* solutes attract or repel at various sites. Extracting intuitive knowledge from atomistic results and developing simplified models for solute-GB interaction is an active field, and there have been many very recent developments [8–12]. Here, we present a physically derived model for solute-GB segregation, which relies on elastic interactions between the solute and excess volume at the GB, as well as a bond-breaking term to represent chemical differences between the bulk and GB environments. This model gives per-site segregation energies rather than simply an averaged boundary result, and comparison with QM/MM and MM results gives physical insight into the dominant mechanisms influencing solute-GB segregation energies. Because the only GB information in the model comes from the *undecorated* GB structure, it is significantly more computationally efficient than even MM calculations when the GB structure has a large number of unique sites.

2. Computational details

2.1. Methods

All QM calculations were performed using the Vienna *Ab Initio* Simulation Package (VASP) [13–16] plane-wave DFT code. We used projector-augmented pseudopotentials [17,18] with the Perdew-Burke-Ernzerhof generalized gradient approximation to the exchange correlation functional [19,20] along with a Methfessel-Paxton smearing [21] of 0.1 eV for the density of states. Ionic and periodic cell degrees of freedom are relaxed to a force-convergence of 0.01 eV/Å by the conjugate gradient method. Using solute-vacancy binding as a test system, we found that *k*-point meshes with 32,000 *k*-points per reciprocal atom (KPPRA) and an energy cutoff of 245 eV provided binding energy results converged to <0.01 eV and a bulk lattice constant of 4.04 Å converged to $<3 \times 10^{-4}$ Å. Further our calculated energy of −0.01 eV (0.40 eV) for Mg-vacancy (Pb-vacancy) binding agrees well with the work of Wolverton [22] which reports −0.02 eV (0.41 eV). These parameters are also applied to the QM-component of our QM/MM calculations. System size convergence is discussed in detail in section 2.2.

For MM calculations, we use the open-source Large-scale Atomic/Molecular Massively Parallel Simulator (LAMMPS) code [23,24] in conjunction with the embedded atom method (EAM) potentials for Al-Mg and Al-Pb by Mendelev et al. [6] and Landa et al. [7], respectively. Both of these potentials have been spatially rescaled to yield precisely the same lattice constant as our DFT results. This is necessary for the QM/MM calculations so that both QM and MM representations of the system relax towards the same crystal structure. After rescaling to this lattice constant, pure Al in the Al-Mg (Al-Pb) potential has a bulk modulus of 80 GPa (74 GPa). While it would be ideal to match both lattice constant and all the elastic properties between quantum and classical representations, we have demonstrated previously [4] that matching the lattice constant is much more significant and the remaining discrepancy in bulk modulus does not introduce substantial error. For QM/MM calculations, the MM components only need to capture Al-Al interaction since the MM calculations of the core region cancel out (see Fig. 1) such that these calculations can be performed by replacing the solute atom with a host atom. To accomplish this we use the rescaled EAM potential of Mendelev—regardless of whether the QM component calculation has a Pb or Mg solute—because its bulk modulus for Al matches the DFT value of 80 GPa. As with DFT, atomic positions in MM calculations are relaxed using the conjugate gradient method to a force convergence of 0.01 eV/Å.

Here we provide only a brief summary of our improved QM/MM method. For an in-depth description of our methodology we direct the reader to our recent work in Ref. [4]. Fig. 1 schematically shows the partitioning of a system into two regions: region I, a small part of the system for which it is desirable to have QM treatment (in our case because of the presence of a solute) and region II, which is much larger but may be sufficiently treated using only MM. The energy of such a coupled system may be represented as [25,26].

$$E_{\mathrm{I+II}} = E_{\mathrm{II}}^{\mathrm{MM}} + E_{\mathrm{I}}^{\mathrm{QM}} + E_{\mathrm{int}}, \tag{1}$$

where superscripts QM and MM indicate whether the energy is calculated using DFT or MM, and subscripts I and II refer to the spatial partitioning of the system. Approximating the interaction energy, E_{int}, with an MM representation [2], this becomes

$$E_{\mathrm{I+II}} \approx E_{\mathrm{I+II}}^{\mathrm{MM}} + E_{\mathrm{I}}^{\mathrm{QM}} - E_{\mathrm{I}}^{\mathrm{MM}} = E_{\mathrm{I+II}}^{\mathrm{QM/MM}}. \tag{2}$$

In Ref. [4] we demonstrated the benefit of adding filler material (shown in grey in the schematic) to eliminate the vacuum surfaces present elsewhere in the literature when cluster calculations are used for region I. Surfaces have a strong and undesirable electronic signal that penetrates deeply into the QM domain, destroying the illusion that it is surrounded by the much larger MM system. Filler material for metallic systems in plane wave codes is thus analogous to the saturation of dangling bonds by hydrogen atoms known to work well for molecular systems [27–29].

To relax the coupled system, the differential of the energy in eq. (2) is taken with respect to atomic positions. For atoms in region II and the core of I, high quality forces are provided by MM and QM representations, respectively. For region I buffer, we follow Liu et al. [3] in the introduction of a correction force to eliminate erroneous surface forces; these atoms are thus relaxed using forces from the MM calculation of region I + II. Filler atoms are always held fixed. The communication between QM and MM representations is mediated by the displacement of atoms under these forces. As in any such displacement-based coupling, there is no strict guarantee of convergence if the QM and MM representations differ substantially [30]. In practice we have not found this to be a significant problem when relaxing our systems such that the forces on each atom among relevant regions (II and I buffer from the MM calculation of the full system, and the core of region I from the QM

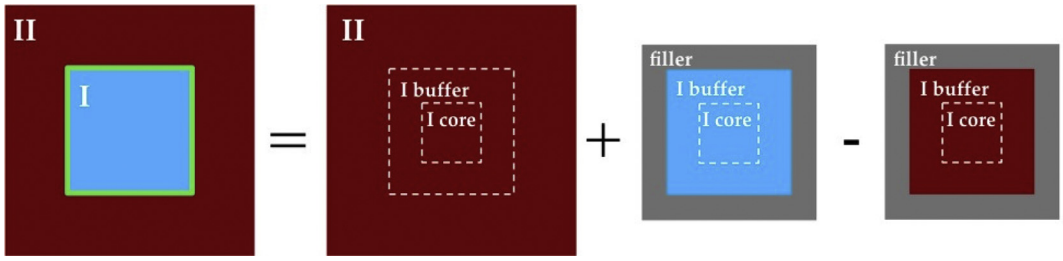

Fig. 1. Schematic representation (not to scale) of system partitioning showing MM (red) and QM (light blue) representations, along with filler material (grey). (For interpretation of the references to colour in this figure legend, the reader is referred to the web version of this article.)

calculation of region I plus filler) are <0.01 eV/Å.

2.2. Systems

To calculate segregation energies to a low-symmetry tilt boundary, we use very large cluster calculations so that the repeat distance of our GB does not have any limit imposed on it by periodic BCs [31]. To generate such a general tilt GB, we begin by creating two large boxes filled with atoms on a face-centered cubic (FCC) lattice with a randomly generated orientation about their [001] axis, and with a translation that is random modulo the size of the Al unit cell. This bulk material does not repeat periodically in our large box, but this is unimportant since we next delete atoms such that only one hemisphere with a radius of 110 Å from each of these two systems remains. The hemispheres are combined into a single system, forming a sphere surrounded by vacuum. Since their original orientations were different, there is now a GB running down the bisecting plane between these hemispheres.

Finding the minimum energy structure for this GB would require searching over all possible translations of one grain relative to the other. For a low-symmetry boundary there is no periodic repeat distance over which such translations become equivalent and such a search is intractable. A useful and efficient approximation to this search is to delete atoms near the interface which sit too close to an atom from the other grain, and then to vary this deletion distance [32]. Such a search is tractable even for general GBs because physically reasonable upper and lower bounds can be chosen for the deletion distance. Since in this study we are interested in per-site segregation energies rather than global GB properties, we chose a single deletion radius rather than performing a complete search. While the overall distribution of local site environments may vary slightly from the minimum-energy boundary a full search would find, we expect to obtain a reasonable approximation of this distribution which samples the space of possible environments well. Thus, as a final step for constructing the boundary, we delete one atom from each pair belonging to different grains that sit within 2 Å of each other, which is <70% of the first nearest-neighbour distance.

Whenever a MM or QM/MM calculation is performed with these spheres, all the atoms in an outer shell with thickness 10 Å (shown in grey) are frozen as fixed BCs. Since this distance is larger than the EAM cut-off, the remaining atoms are unaware of the vacuum surface. We fully relax all non-frozen atoms using the rescaled potential of ref. [6] prior to any QM/MM calculations. The resulting structure four our low-symmetry GB can be seen [33] in Fig. 2. It has a relative misorientation between the two grains of 23.77°, which lies between the 22.62° of the Σ13 CSL boundary and 25.06° of the Σ85 CSL boundary. Since only a small deviation is necessary to destroy coincidence, this boundary is completely general. GB sites (light green) were identified before this relaxation using common neighbour analysis [34,35]. The four sites chosen for QM/MM calculation from near the center of the cluster are shown enlarged with a variety of colours. Part (b) of the figure shows their local environment and relative positions in more detail.

As is common in periodic DFT calculations of segregation energies, we use four separate calculations to compare the system with the solute at the GB site and infinitely separated. Using the convention that positive energy represents favourable segregation, this reads

$$E_{\mathrm{seg}} = \left(E_{\mathrm{GB}} + E^{X}_{\mathrm{bulk}}\right) - \left(E^{X}_{\mathrm{GB}} + E_{\mathrm{bulk}}\right), \tag{3}$$

where the subscript indicates the structure of the host material, and the presence or absence of the superscript indicates whether or not a host atom is replaced with the solute species *X*. For QM/MM and MM calculations of segregation energies, we also use a cluster of bulk Al which is treated in a similar manner as the general tilt boundary apart from the presence of the GB. The contributions to the segregation energies from the fixed BC surfaces of these large clusters thus cancel out.

In addition to the general tilt boundary, we also perform QM/MM, MM, and periodic QM calculations at the symmetric (310) [001] Σ5 tilt boundary. This boundary repeats over a short enough distance to be accommodated by periodic BCs, but for QM/MM and MM calculations another cluster is constructed, as described above.

When placing large substitutional solutes, such as Pb, into a comparatively small host, like Al, it is critically important to consider convergence with respect to system size. For the size of our periodic DFT cells and also the size of region I with periodic BCs in QM/MM calculations, this has already been investigated in our previous work [4]. There, we used a less expensive ultra-soft pseudopotential (USPP) which allowed us to study QM calculations using in excess of 1500 atoms.

For periodic DFT, we use a bulk structure made of 4 × 4 × 4 repeats of the four-atom unit cell for a total of 256 atoms, and our GB structure repeats the Σ5 kite structure four times (18.0 Å), as well as having two atomic planes along the [001] axis (8.0 Å), and a grain thickness of 23.1 Å for a total of 400 atoms. These structures gave Mg-GB (Pb-GB) segregation energy at the planar GB site converged to 0.01 eV (0.02 eV) with respect to larger cells when using the USPP [4].

For QM/MM calculations, it is important to check convergence with respect to the size of region I. We construct this region by selecting a site or sites of interest (e.g. the GB site at which a solute will be placed) and building consecutive shells of nearest neighbours, thus isolating it as efficiently as possible from the buffer-filler and filler-filler interfaces (the latter resulting from the periodic BCs.) Further, we take filler atom positions from the *initial* positions of the larger region I + II superstructure in order to minimize the impact of the filler-buffer interface. Using the USPP with two such neighbour shells to make the core of region I, we tested the convergence of Mg and Pb binding to a vacancy and

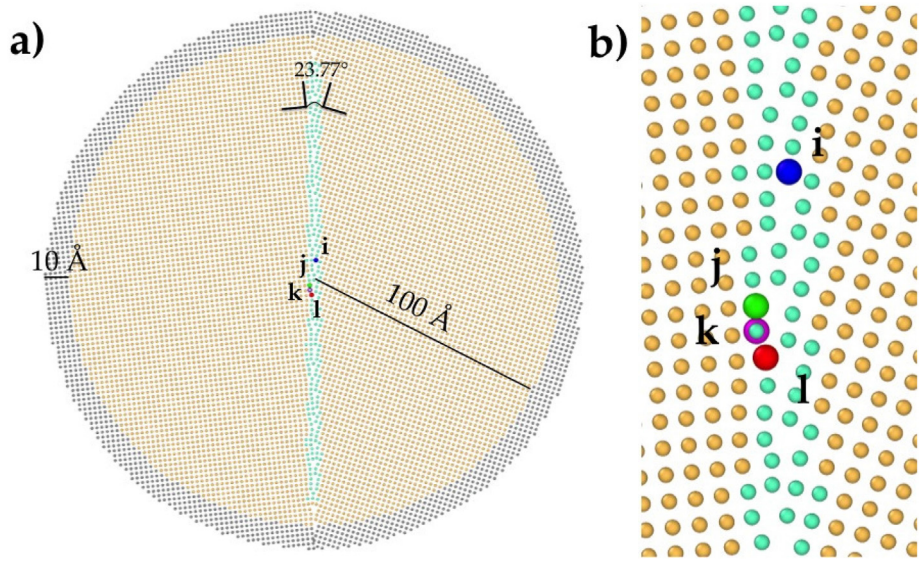

Fig. 2. Region I + II superstructure for the general tilt boundary, shown for a slice looking down the [001] axis for (a) the entire cluster, and (b) a smaller region near the sites **i-l** sampled by QM/MM. Fixed BCs shown in grey, bulk sites in yellow, GB sites in light green, and sites used for QM/MM segregation calculations shown large in various colours with labels. (For interpretation of the references to colour in this figure legend, the reader is referred to the web version of this article.)

segregation to the planar site of the Σ5 GB. We found that a single buffer shell gave binding and segregation energies converged to within 0.05 eV in all four cases [4].

We also use systems with two core shells and one buffer shell here, which can be seen after QM/MM relaxation for the undecorated Σ5 boundary in Fig. 3(a–c), and for the undecorated general tilt boundary in Fig. 4 with core atoms shown in light blue, buffer atoms in dark red, and fixed filler atoms in grey. Enlarged atoms show where solutes will be placed. The influence of Mg and Pb on local structure are shown for the Σ5 GB in Fig. 3(d–f) and (g-i), respectively, with arrows showing the effect of relaxation exaggerated by a factor of ten. The benefit of choosing filler atom positions from the initial positions of the MM-relaxed structure is clear, since even after QM/MM relaxation in the presence of these over-sized solutes the interface between buffer and filler atoms is not easily discernible. The filler-filler interface is thus the coupling artefact with the strongest perturbative influence on the electronic environment of region I core. We also note that while slices are used to show these domains, we do not make use of periodicity in the [001] direction; region I is a cluster surrounded by filler in all three dimensions, allowing this method to be applied with equal ease to GBs with multiple axes of misorientation.

Lastly, we have also examined convergence with respect to the size of the large cluster using MM. Testing segregation to all three unique sites at the Σ5 boundary for both Pb and Mg, increasing the cluster radius from 110 Å to 210 Å gives the same segregation energies to 0.01 eV.

3. Results

To begin, we re-demonstrate the validity of our QM/MM coupling scheme by comparison to the gold-standard of periodic DFT for all three unique sites at the Σ5 GB. When plotted in Fig. 5(a) against pure DFT results, E_{seg}^{QM}, we find that the QM/MM segregation energies, $E_{seg}^{QM/MM}$, are accurate over a wide energetic range (including a repulsive site) for both solutes. For Mg, agreement is nearly perfect, with a mean (maximum) error of 0.02 eV (0.03 eV) and a standard deviation of <0.01 eV for $E_{seg}^{QM/MM} - E_{seg}^{QM}$. For Pb, the mean (maximum) difference is only somewhat larger at 0.05 eV (0.08 eV), as is the standard deviation of 0.04 eV. It is not surprising that the QM/MM method performs worse for Pb, since this element is both more electronically complex than Mg and also significantly larger, making it more sensitive to imperfections in the QM/MM treatment of the electronic state and strain energy.

Overall, the performance of the QM/MM method is excellent; taking all six data points from both solutes together, it yields a mean difference and standard deviation of 0.04 eV and 0.03 eV, respectively. The agreement with full QM could be systematically improved by increasing the size of the core and buffer subdomains. Since the QM-component calculations of region I + filler already consist of 437, 499, and 494 atoms for sites a, b, and c, this is not a feasible approach given current computational power—although it may become possible in the future.

Based on these results for the symmetric Σ5 GB, where direct comparison to periodic DFT is possible, we expect the QM/MM method to return segregation energies of similar quality at the general tilt boundary, where a pure QM calculation is currently impossible. The QM/MM segregation energies for both solutes at both boundaries are shown plotted against the excess Voronoi volume [36] of the undecorated GB site in Fig. 6. To the best of the authors' knowledge, these are the first QM-based segregation energies calculated for a low-symmetry GB. Both solutes show a trend of stronger segregation to larger sites, which can be understood from the excess site volume relieving strain imposed by these oversized solutes. Numerical values for QM/MM segregation energies for the general tilt sites in Fig. 2 can be found, along with other data, in the supplementary material.

Another interesting application of QM/MM calculations is to test the performance of empirical potentials. Since EAM potentials are frequently fit to DFT data, here we have the possibility to compare them against QM-based calculations for which they were certainly not fit. In the future, this type of multiscale method may also provide new data sets with which to generate improved potentials. MM segregation energies E_{seg}^{MM} obtained from the rescaled Al-Mg and Al-Pb potentials are plotted against QM/MM results, $E_{seg}^{QM/MM}$, for both GBs in Fig. 7(a). For Mg (Pb), the maximum, mean, and standard deviation in the difference between methods are 0.17, 0.04, and 0.08 eV (−0.30, −0.11, and 0.09 eV), respectively. The only

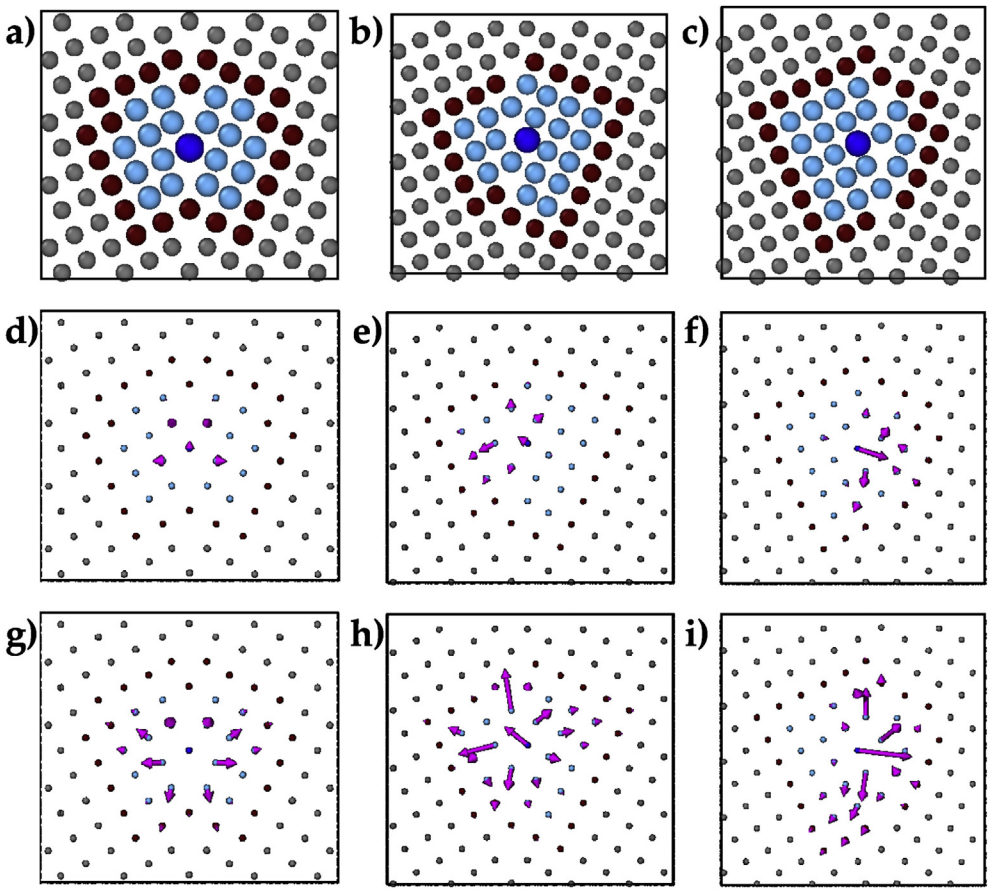

Fig. 3. A slice of region I + filler relaxed by QM/MM for Σ5 GB sites **a**, **b**, and **c** is shown looking down the shared [001] axis of both grains. (a)–(c) show the QM/MM-relaxed undecorated structure with enlarged sites where solutes are placed. The remainder of the core sub-region is shown in light blue, the buffer is dark red, and filler atoms are grey. The black box shows the boundaries of the periodic cell. (e)–(f) contain arrows indicating displacements during relaxation in the presence of Mg at each of the three GB sites. (g)–(i) are similar for Pb. In all cases the arrows exaggerate displacements by one order of magnitude. (For interpretation of the references to colour in this figure legend, the reader is referred to the web version of this article.)

MM predictions in apparent qualitative disagreement with QM/MM results—predicting repulsion instead of attraction or vice versa—are for Mg at site **j** and Pb at site **i**. In both cases, these points are within 0.10 eV of the origin, i.e. they are within the noise we observe in the relative energies. Thus, qualitative differences may occur without any fundamentally different treatment of the physics.

Both MM potentials accurately capture the overall trends in segregation, although the Al-Pb potential performs worse and systematically underestimates the QM/MM results. This underestimate may be partially explained by recalling that the Al-Al interactions in the Al-Pb potential produce a weaker Al bulk modulus than both QM and the Al-Mg potential (which is used for Al-Al interactions in regions II and I buffer of the QM/MM calculations.) Because the Pb atom is surrounded by "softer" Al atoms in this pure MM calculation than in the QM/MM calculation, the over-sized Pb atom will have less elastic strain energy relieved by moving to the GB, which has excess local volume for most sites.

QM/MM solute-GB segregation energies can also be studied for insight into physical mechanisms underlying solute segregation at general boundaries. In one of the earliest models for solute-GB segregation, McLean [37] proposed the approximation that the elastic strain induced by a substitutional solute is completely relieved by moving the solute to the GB. More recently, some of the present authors have proposed a simple linear elastic model for predicting per-site segregation energies through the interaction of solute pressure and the local site volumes [38]. For a solute X at a GB site i, the model takes the form

$$E_{\text{seg}}^{\text{Elast}} = P_X \Delta V^i, \tag{4}$$

where the site volume difference ΔV^i is simply the difference between Voronoi volumes of the ith GB site and the bulk. The solute pressure, P_X, is approximated using the host bulk modulus, B, and the excess volume of the solute calculated from the volumes of relaxed bulk supercells with the solute, V_{bulk}^X, and without it, V_{bulk}:

$$P_X = B\frac{V_{\text{bulk}}^X - V_{\text{bulk}}}{V_{\text{bulk}}}. \tag{5}$$

In Ref. [38], we found that this model worked well for predicting the segregation energies of a wide variety of over-sized and under-sized solutes to a Σ7 GB in Mg. Its performance was weak at sites with $\Delta V^i \approx 0$, and did not work well at any site for the solutes Zr and Ti.

Here, we test this model using a QM-calculated solute pressure term, which is 0.15 eV/Å^3 (0.58 eV/Å^3) for Mg (Pb) in Al, and site volumes from the superstructure relaxed by the potential in Ref. [6]—i.e. the initial positions of QM/MM calculations. Model results are shown plotted against corresponding QM/MM values in Fig. 7(b). For Mg-GB segregation, the elastic model is quite successful in capturing the trends in segregation from site to site, with

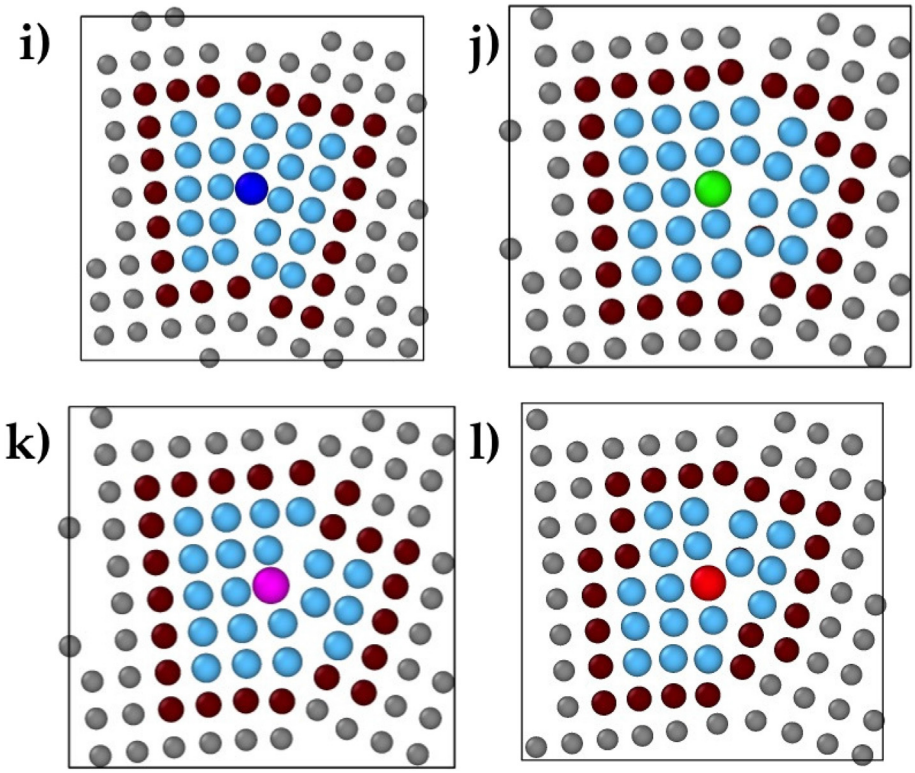

Fig. 4. A slice of region I + filler relaxed by QM/MM for general tilt GB sites **i-l** is shown looking down the shared [001] axis of both grains. The structure is undecorated, but enlarged sites show where solutes are placed. The remainder of the core sub-region is shown in light blue, the buffer is dark red, and filler atoms are grey. (For interpretation of the references to colour in this figure legend, the reader is referred to the web version of this article.)

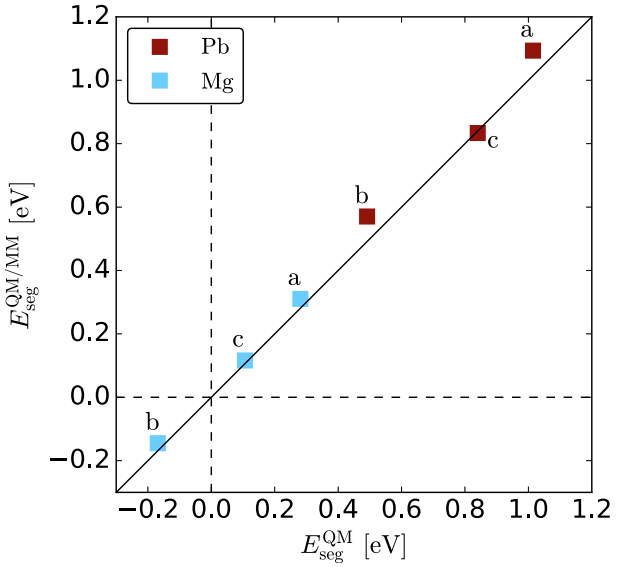

Fig. 5. QM/MM segregation energies for Mg (light blue) Pb (dark red) at sites along the Σ5 GB compared to QM results. A solid black line shows perfect agreement. Letters map segregation energies to sites shown in Fig. 3(a–c). (For interpretation of the references to colour in this figure legend, the reader is referred to the web version of this article.)

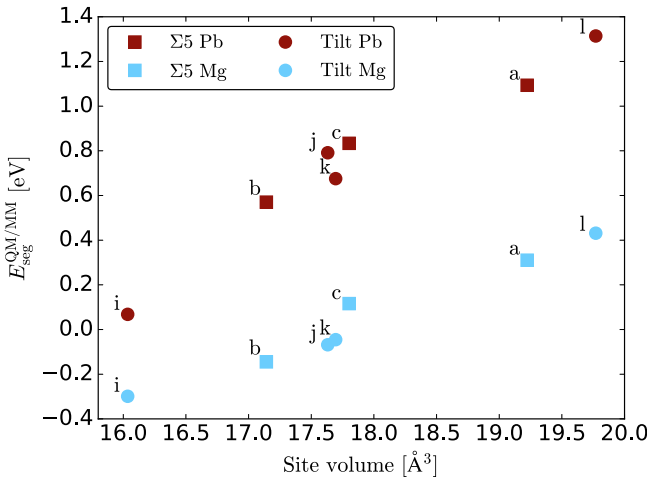

Fig. 6. Segregation energies for Mg (light blue) and Pb (dark red) at sites along the Σ5 GB (squares) and general tilt GB (circles). Energies are plotted against the local Voronoi volume of each undecorated GB site. Letters map segregation energies to sites shown in Figs. 3 and 4. (For interpretation of the references to colour in this figure legend, the reader is referred to the web version of this article.)

a slope near unity and a small scatter as indicated by the standard deviation of 0.07 eV for the energy difference. The attraction of Mg to "looser" GB sites in Al compared to "tighter" sites has been observed qualitatively elsewhere [8,9,39]; here we provide a physically motivated quantification of this effect. However, a mean deviation of 0.20 eV above QM/MM segregation energy drives many of the sites to be incorrectly predicted as attractive.

For Pb-GB segregation, the elastic model produces reasonable energies for only a few of the sites, while others are incorrect. The model does, however, provide nearly perfect ordering for the strength of segregation among the sites, which indicates that an elastic interaction between the solute and local site volume plays an important role in Pb-GB segregation. However, this interaction

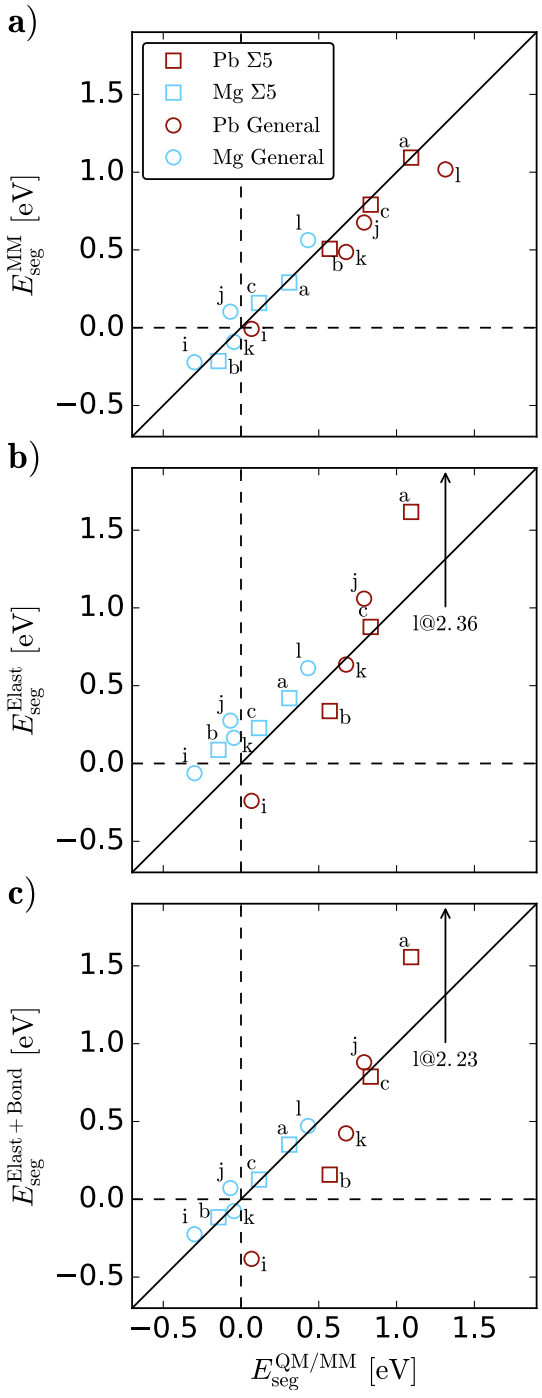

Fig. 7. Segregation energies for Mg (light blue) and Pb (dark red) at sites along the Σ5 GB (squares) and general tilt GB (circles). Energies calculated by (a) MM using the rescaled EAM potentials of refs. [6] and [7], (b) the elastic model, and (c) the full elastic plus bonding model are all compared to QM/MM results. A solid black line shows perfect agreement with QM/MM. Letters map segregation energies to sites shown in Figs. 3 and 4. (For interpretation of the references to colour in this figure legend, the reader is referred to the web version of this article.)

does not vary linearly with a slope given by our approximation to the pressure of Pb on the host matrix.

While excess volume at the GB is an important predictor for the segregation of over-sized substitutional solutes like Pb and Mg, one may also consider differences in the state of bonding at the GB [40], which we characterize here using the coordination number, N_c:

$$E_{seg}^{Bond} = E_{bond}\Delta N_c^i, \tag{6}$$

where $\Delta N_c^i = N_c^i - N_c^{bulk}$ is the difference between the coordination number at the ith GB site and the bulk coordination number, and E_{bond} is the energy per bond change. For the solute segregation described by eq. (3), a solute in the bulk trades places with a host atom at the boundary. In this simplified bonding model, solute segregation to a site with $\Delta N_c^i < 0$ thus requires breaking ΔN_c^i host-solute bonds and forming the same number of host-host bonds. To evaluate this energy per bond, we consider the solute's energy of solvation, E_{solv}^X, and divide by 12—the number of nearest neighbours in FCC Al. Because we already treat the elastic interaction another way, we approximate the bond energy using unrelaxed solvation energies. These energies are calculated from DFT using

$$E_{solv}^X = E_{bulk}^X - E_{bulk} - E_X, \tag{7}$$

where the two bulk superstructure energies, E_{bulk}^X and E_{bulk}, with and without the substitutional solute, respectively, are also necessary for the calculation of P_X, and the remaining energy of the isolated solute atom, E_X, is very inexpensive to calculate. For Mg and Pb, the resulting unrelaxed solvation energies are −1.39 eV and −1.23 eV, respectively. The energies for breaking a host-solute bond and replacing it with a host-host bond, E_{bond}, are thus 0.12 eV and 0.10 eV for Mg and Pb, respectively.

To calculate the coordination number under the low-symmetry conditions found at a GB, we follow Huang et al. [41] in the use of a Fermi-Dirac function with a smearing parameter σ such that

$$N_c^i = \sum_j f(r_{ij}), \tag{8}$$

where the sum on j runs over all other atoms sitting a distance r_{ij} from the ith site, and

$$f(r) = \frac{1}{1 + \exp\left(\frac{r - r_0}{\sigma}\right)}. \tag{9}$$

We use half the distance between the first- and second-nearest-neighbours (1NN and 2NN) for $r_0 = 3.45$ Å, and a smearing parameter $\sigma = 0.22$ Å—approximately 20% of the distance between the 1NN (2.86 Å) and 2NN (4.04 Å) distances. In this way, neighbours of each site contribute to the total coordination number in a continuous manner. In the bulk, 1NN atoms under-contribute to N_c, adding only 0.94 instead of 1, but 2NN atoms contribute 0.06 instead of 0. One result of this smearing is that the bulk coordination number is not exactly 12; using $\sigma = 0.22$ eV, we obtain $N_c^{bulk} = 11.64$. Because the contribution from distant neighbours decays exponentially, the computational cost for evaluating N_c^i at n sites is only $\mathcal{O}(n)$.

The result of combining the bonding model with the elastic model is shown in Fig. 7(c). Despite its simplicity, this combined model predicts Mg-GB segregation extremely well, with the maximum, mean, and standard deviations of the energy difference as 0.14, 0.04, and 0.05, respectively. This superb agreement is a strong indication that all of the important physics for Mg-GB segregation in Al is well captured by a combination of a $P\Delta V$ description and a bond-breaking argument. Bond order potentials, e.g. the Finnis-Sinclair-type EAM potential from Ref. [6], use a sub-linear scaling for the electron density embedding term, typically a power of 0.5. While a similar sub-linear counting of broken bonds may be more physical, we find that our linear simplification performs well, perhaps because linearity is a good approximation over the relatively small range of coordination changes that we observe,

namely −2.7 to 0.2.

For Pb, adding bond breaking does not have any significant effect, although it does bring the predicted segregation energy at sites **j** and **c** closer to the correct ordering. However, even with this improvement the model can provide only qualitative information about trends in segregation energy for Pb. While the final relaxed state differs from the original configuration for both solutes, we see in Fig. 3(d–f) and (g-i) that local rearrangements due to Pb are much more significant for Pb than for Mg. We will demonstrate later that this relaxation in the presence of the solute plays a critical role in the model's success or failure to predict the segregation energy.

In the same way we relied on QM/MM segregation energies as a standard after confirming that they give a good reproduction of QM results, the good performance of the MM calculations shown in Fig. 7(a) suggests that we can use MM as a standard for further testing the simpler physically-based models for Mg-GB interaction. The dramatically reduced cost of MM calculations compared to any calculation involving QM opens many more sites for examination. A slice of the 2480 GB sites lying in a disc with a radius of 50 Å centered in the middle of the cluster is shown in Fig. 8(a), coloured by the Mg-GB segregation energy given by MM. Mg segregation energies to these sites range from −0.32 to 0.60 eV, but are on average weakly favourable, as shown in the energy distribution plot of Fig. 8(b). Alongside these, we also show distributions for (c) site Voronoi volumes—which roughly follow a log normal distribution, as observed for Mg [38]—and (d) site coordination number, N_c^i.

We compare Mg segregation energies calculated by the fit-free, physically based models from eqs. (4) and (6) to MM calculations in Fig. 9. Both models capture overall trends in the segregation energy. Adding the bonding term changes an average overestimate to an underestimate, but also, more importantly, reduces the variance of the model such that the maximum, mean, and standard deviation of the energy difference go from 0.46, 0.07, and 0.14 eV for the pure elastic model in Fig. 9(a) to 0.40, −0.05, and 0.09 eV for the combined elastic and bonding model. In addition to providing useful physical insight into the underlying mechanisms for Mg-GB segregation, the combined elastic plus bonding model provides quantitatively reasonable predictions for a large majority of GB sites, giving results within ±0.10 eV for most sites. Because of the wide variety of local structures at this general tilt GB, we expect such a model to perform well for Mg segregation to other structural defects in Al, e.g. dislocation cores, under similarly dilute conditions.

To better understand the conditions under which the model performs poorly, we have plotted all of the GB sites in coordination-volume space in Fig. 10(a) with all the sites for which model predictions deviate by more than 0.10 eV from MM values shown as dark red triangles. We see here that these problematic sites are not easily separable in the space in which our model exists. It is not simply failing, e.g., at very large sites, or sites which are over-coordinated. This figure also demonstrates that while the

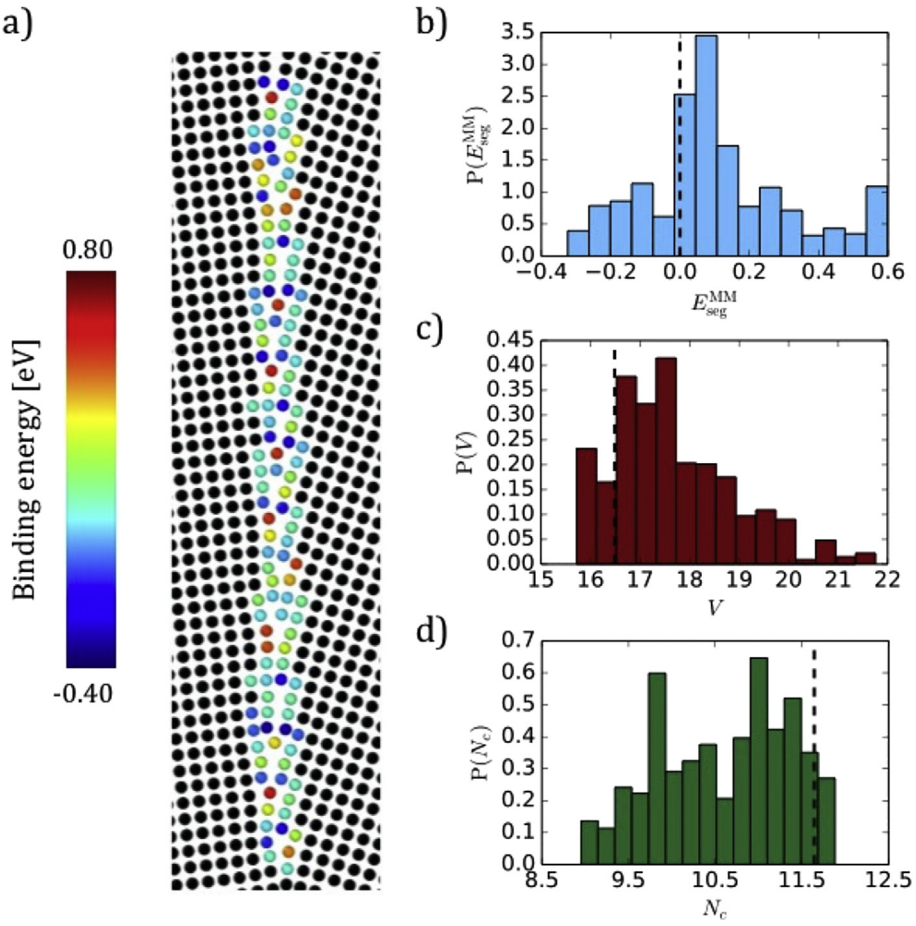

Fig. 8. (a) Slice of the tilt boundary with GB atoms coloured by Mg-GB segregation energy, as calculated by MM. (b–d) Probability distributions for Mg-GB segregation energy, GB site Voronoi volume, and GB site coordination number. Dashed lines represent zero-segregation energy, bulk site volume, and bulk coordination number, for (b), (c), and (d) respectively. (For interpretation of the references to colour in this figure legend, the reader is referred to the web version of this article.)

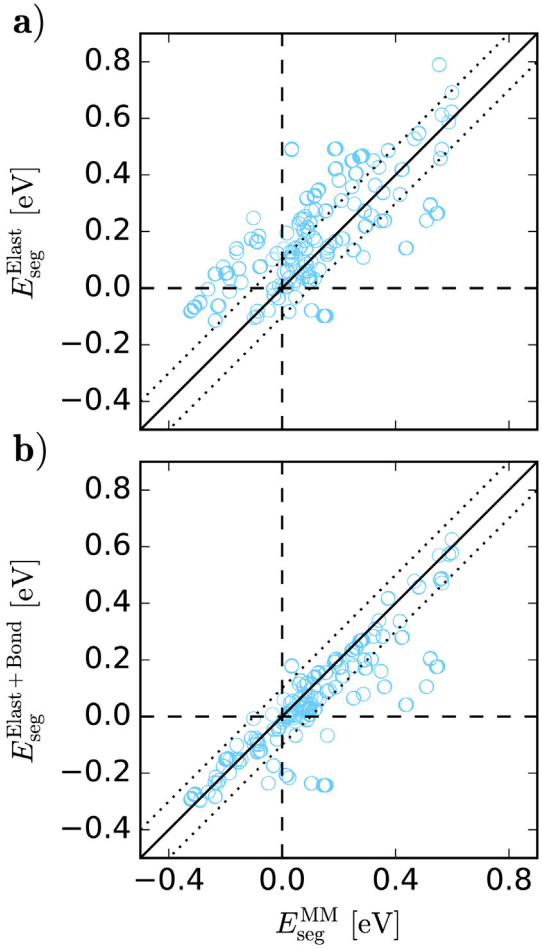

Fig. 9. Mg-GB segregation energies for sites in the general tilt boundary by (a) elastic model, and (b) combined elastic and bonding model plotted against segregation energies calculated with MM. Dotted lines in (b) show a window of ±0.10 eV agreement.

distributions of V and N_c in Fig. 8(c) and (d) roughly mirror each other, this is not because every site with excess volume is undercoordinated; in fact there is only a weak anti-correlation between these two properties on a per-site basis.

In Fig. 10(b) we look at the difference in ΔV^i and ΔN_c^i before and after relaxation in the presence of an Mg atom placed at the ith site. In this space, we do see good separation of problematic sites; the majority undergo significant changes in either local volume or coordination during relaxation. Although the host atoms also relax in the presence of Mg in the bulk environment, there are some GB sites at which this relaxation is much more pronounced. This effect is completely missed by our linear elastic model, which supposes that all of the strain relief comes only from the excess volume of the undecorated site. (An analogous argument can be made for the linear bonding model.) For these sites which relax so differently from the bulk, undecorated values of ΔV^i and ΔN_c^i are no longer reliable model parameters. While this provides an understanding of what is causing model failure, we do not currently have a method for identifying these problematic sites *a priori*—they are found here only after explicitly running an MM calculation.

We have also compared the combined model to MM results for Pb, shown in Fig. 11, where MM energies range from −0.18 to 3.54 eV. The Al-Mg and Al-Pb potentials treat the Al-Al interaction differently, and the resulting GB structure relaxed by the Al-Pb potential has several kites which do not have a clean, consistent

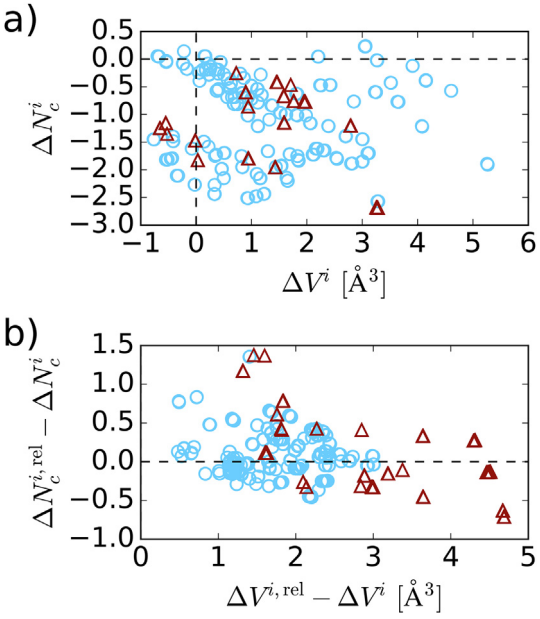

Fig. 10. Locations of GB sites in (a) coordination-volume space and (b) changes in the coordination and volume after relaxation with an Mg atom at the site. Sites for which the model prediction for Mg-GB segregation energy disagrees with MM results by 0.10 eV or more are shown as dark red triangles. (For interpretation of the references to colour in this figure legend, the reader is referred to the web version of this article.)

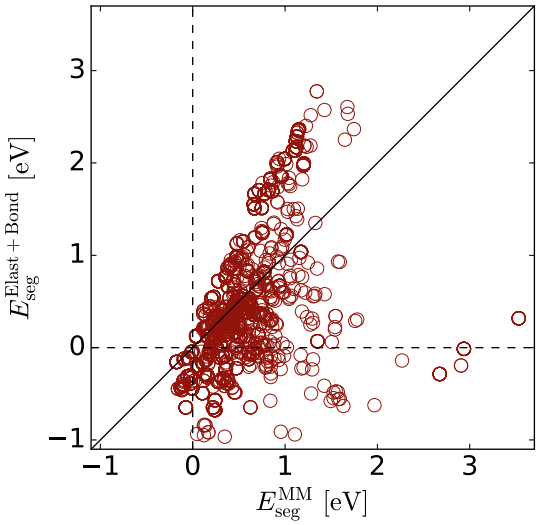

Fig. 11. Pb-GB segregation energies for sites in the general tilt boundary from the combined elastic and bonding model plotted against results from MM calculations.

structure along the [001] axis. This was not an issue for sites **i-l**, whose kites were qualitatively similar to those relaxed by the Al-Mg potential, but for some other kites this results in a wider variety of local environments for a solute atom to experience. When comparing model predictions to Pb-GB segregation energies generated by the rescaled Al-Pb potential, we use the undecorated structure relaxed *by that potential* as a source for site volumes and coordination numbers; this is the reason that there appears to be much more data in Fig. 11 than in Fig. 9. In order to explore the possible effect of these Al-Al interactions, we have also performed segregation energy calculations using MM/MM coupling, as described in the supplementary material.

For Pb, we find that the model is only capable of giving a broad,

qualitative description and does not demonstrate the sort of quantitative accuracy found for Mg-GB segregation. Because Pb is much larger than Mg—more than twice as large as Al, as opposed to ~30% larger—the changes in local structure after relaxation are more extreme, as seen in Fig. 3. In Fig. 12 we demonstrate the quantitative effect of these relaxations by plotting errors in the model prediction as a function of the relaxation volume. For both solute species, the amount of relaxation due to the solute varies from site to site. For Mg the dependence of the model error on this relaxation volume is weak, but for sites which relax by more than ~3 Å^3 the model consistently under-predicts the segregation energy, an observation consistent with Fig. 10(b). For Pb the model error depends approximately linearly on the amount of solute-induced relaxation. One explanation for this is that Pb's very large size means that "rigid" sites which permit less relaxation than a bulk site are strongly penalized, while very "soft" sites which allow a large amount of relaxation are very favourable—even though their undecorated size may be only moderate. If this capacity for relaxation could be predicted prior to the full solute-GB MM calculation, a corresponding correction term could be added to the existing model. Such a correction would bring the quality of Pb-segregation energy predictions significantly closer to the quality of those obtained for Mg. Until then, the elastic and bond-breaking model presented here will be most useful for substitutional solutes with roughly the same size as the host material.

Finally, we note that the quality of the model performance for Mg does not depend strongly on the choice of the smearing parameter. Its exact value was obtained by minimizing the root mean square error of model predictions to the MM Mg data set using P_X and E_{bond} as tunable parameters, along with allowing for a constant shift. Finding ΔN_c^i using a value of $\sigma = 0.22$ Å minimized the fit error, but a broad range of smearing parameters from $\sigma = 0.1$ Å to $\sigma = 0.3$ Å—which covers ~10–25% of the distance between 1NN and 2NN—give no qualitative difference in the fit model. Over this range, quantitative differences for fit values of P_X and E_{bond} are less than 0.02 eV/Å^3 and 0.05 eV/bond, respectively. Qualitative differences emerge when σ is set to be exceptionally small (e.g. 0.02 Å where the transition is nearly a step function), or large (e.g. 0.5 Å where smearing gives significant weight to 2NN atoms and beyond.) For Pb, no choice of σ, nor any choice of P_X or E_{bond}, was found to qualitatively improve the model performance; i.e. for Pb there does not exist a good linear model in the space of $(\Delta V^i, \Delta N_c^i)$.

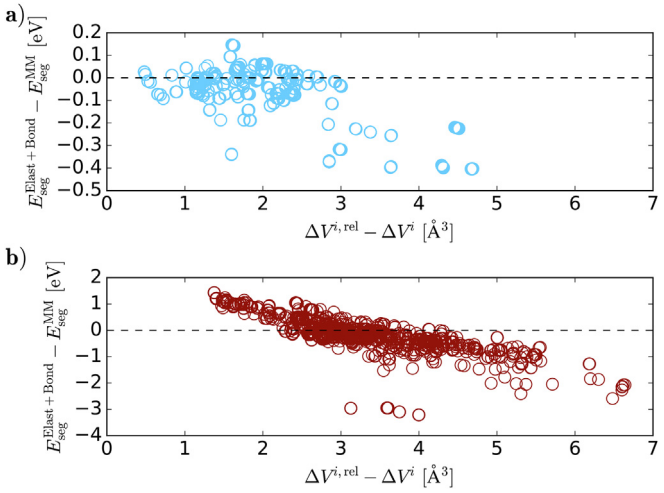

Fig. 12. Errors in model energy as a function of the relaxation volume in the presence of a solute for (a) the presence of Mg using the potential from Ref. [6] in blue, and (b) the presence of Pb using the potential from Ref. [7] in red. (For interpretation of the references to colour in this figure legend, the reader is referred to the web version of this article.)

4. Conclusion

Mg- and Pb-segregation energies to all three unique sites at a (310)[001] Σ5 tilt GB in Al were calculated using the QM/MM multiscale technique described in Ref. [4] and compared to traditional, periodic DFT results. The QM/MM method performed well for each of the six site-solute combinations, and overall QM/MM segregation energies had a standard deviation of 0.03 eV and a small offset of 0.04 eV compared to DFT results. Four further segregation energies were calculated for each solute, this time at the general [001] tilt boundary described in section 2. To the best of the authors' knowledge, this is the first QM-based investigation of solute segregation to a low-symmetry boundary. Because the multiscale technique here does not rely on periodicity of the structure in any direction, such calculations are feasible for any structure which can be represented in MM but which has some localized defect requiring QM-level treatment, e.g. solute or vacancy interaction with GBs, dislocation cores, or other structural defects. It is important to note that the QM/MM method only requires the EAM potential for the host system and not that of the host-solute system.

QM/MM results were used to evaluate the performance MM calculations using existing Al-Mg [6] and Al-Pb [7] EAM potentials which were rescaled to exactly match the DFT lattice constant. The Al-Mg potential performed well, reproducing QM/MM segregation energies with a standard deviation of 0.08 eV and a small offset of 0.04 eV when comparing all seven sites. While the Al-Pb potential accurately reproduced trends in Pb-GB segregation energy across various sites, with a standard deviation in the energy difference of only 0.09 eV, its performance was somewhat worse than the Al-Mg potential; EAM predictions for Pb-GB segregation energy consistently underestimated QM/MM results, and the mean (maximum) deviation was −0.11 eV (−0.30 eV). This maximum deviation is significant not only in absolute terms, but is also a large relative error, giving a total MM segregation energy for Pb to site **l** that is only 78% of the QM/MM value.

Lastly, we investigated the physics underlying solute-GB segregation by testing a physical model which includes an elastic interaction and a bond-breaking term. The elastic interaction takes a simple $P\Delta V$ form, where the pressure induced by a size-mismatched solute interacts with site-specific volume differences. The bond counting term uses the solvation energy to approximate the energy per 1NN bond and scales this by the change in the coordination number at the site compared to the bulk. We stress that this model does not contain fitting parameters, but is physically-based. There is an *ad hoc* choice of a smearing parameter for calculation coordination numbers, but results are insensitive to its choice over a large, physically intuitive range. Calculating the solute pressure and solvation energy using QM introduces some computational overhead, but once this is complete the segregation energies to every site at a grain boundary can be computed in only seconds using a single MM calculation for the undecorated boundary. For sufficiently large systems, this overhead compares favourably to the time required for explicitly performing many MM calculations with a solute at each site. Because solute properties come from QM calculations, this model can also be used to predict segregation energies at GBs for solutes for which no host-solute classical potential exists.

This model predicted Mg-GB segregation energy exceptionally well, with good agreement to QM/MM results at a few selected sites, and to MM calculations at a much broader selection of sites.

When comparing to MM Mg-GB segregation energies across 2480 sites, the combined model had a mean difference and standard deviation of only −0.05 eV and 0.09 eV, respectively. This is comparable to the level of agreement found between the MM and QM/MM results for the seven sites at which data was available. The quality of the agreement indicates that these two energetic terms, elastic and bond-based, represent the significant physics in Mg-GB interactions. We expect that such a model should work well for Mg interaction with other spatial defects in Al under dilute conditions. The model was found to perform less well for sites at which there is significant changes in the GB structure under relaxation in the presence of a solute, but at present no method is proposed for identifying these sites *a priori*.

For Pb, the model performed poorly. While the nearly-monotonic relationship between site volume and QM/MM segregation energy indicates that Pb's large size plays a dominant role in Pb-GB interaction, our linear model does not capture the form of this interaction. Further, the introduction of a bond counting term had little effect on the overall quality of predictions. The failure of the physically-motivated model to describe Pb, and the less than ideal performance of the EAM potential for the same solute both emphasize the utility of QM/MM methods for providing insight into systems whose structure is too complex for traditional DFT and whose complex behaviour stretches the limits of simpler descriptions.

Acknowledgements

The authors would like to acknowledge WestGrid/Compute Canada for providing computational resources. LH was supported in part by an Alexander Graham Bell Post-Graduate Scholarship from the Natural Sciences and Engineering Research Council of Canada (NSERC). This project has received funding from the European Research Council (ERC) under the European Union's Horizon 2020 research and innovation programme (Grant Agreement No. 639211).

Appendix A. Supplementary data

Supplementary data related to this article can be found at http://dx.doi.org/10.1016/j.actamat.2017.04.024.

References

[1] P. Lejček, M. Šob, V. Paidar, V. Vitek, Why calculated energies of grain boundary segregation are unreliable when segregant solubility is low, Scr. Mater 68 (2013) 547–550.
[2] N. Choly, G. Lu, E. Weinan, E. Kaxiras, Multiscale simulations in simple metals: a density-functional-based methodology, Phys. Rev. B 71 (2005) 094101.
[3] Y. Liu, G. Lu, Z. Chen, N. Kioussis, An improved qm/mm approach for metals, Model. Simul. Mater. Sci. Eng. 15 (2007) 275.
[4] L. Huber, B. Grabowski, M. Militzer, J. Neugebauer, J. Rottler, A qm/mm approach for low-symmetry defects in metals, Comput. Mater. Sci. 118 (2016) 259–268.
[5] B. Grabowski, T. Hickel, J. Neugebauer, Ab initio study of the thermodynamic properties of nonmagnetic elementary fcc metals: exchange-correlation-related error bars and chemical trends, Phys. Rev. B 76 (2007) 024309.
[6] M. Mendelev, M. Asta, M. Rahman, J. Hoyt, Development of interatomic potentials appropriate for simulation of solid–liquid interface properties in al–mg alloys, Philos. Mag. 89 (2009) 3269–3285.
[7] A. Landa, P. Wynblatt, D. Siegel, J. Adams, O. Mryasov, X.-Y. Liu, Development of glue-type potentials for the al–pb system: phase diagram calculation, Acta Mater 48 (2000) 1753–1761.
[8] H. Wang, M. Kohyama, S. Tanaka, Y. Shiihara, First-principles study of si and mg segregation in grain boundaries in al and cu: application of local-energy decomposition, J. Mater. Sci. 50 (2015) 6864–6881.
[9] L. Karkina, I. Karkin, A. Kuznetsov, I. Razumov, P.A. Korzhavyi, Y.N. Gornostyrev, Solute–grain boundary interaction and segregation formation in al: first principles calculations and molecular dynamics modeling, Comput. Mater. Sci. 112 (2016) 18–26.
[10] M. Gong, F. Liu, Y. Chen, Modeling solute segregation in grain boundaries of binary substitutional alloys: effect of excess volume, J. Alloys Compd. 682 (2016) 89–97.
[11] M.A. Gibson, C.A. Schuh, A survey of ab-initio calculations shows that segregation-induced grain boundary embrittlement is predicted by bond-breaking arguments, Scr. Mater 113 (2016) 55–58.
[12] X. Wu, Y.-W. You, X.-S. Kong, J.-L. Chen, G.-N. Luo, G.-H. Lu, C. Liu, Z. Wang, First-principles determination of grain boundary strengthening in tungsten: dependence on grain boundary structure and metallic radius of solute, Acta Mater 120 (2016) 315–326.
[13] G. Kresse, J. Hafner, Ab initio molecular dynamics for liquid metals, Phys. Rev. B 47 (1993) 558.
[14] G. Kresse, J. Hafner, Ab initio molecular-dynamics simulation of the liquid-metal–amorphous-semiconductor transition in germanium, Phys. Rev. B 49 (1994) 14251.
[15] G. Kresse, J. Furthmüller, Efficiency of ab-initio total energy calculations for metals and semiconductors using a plane-wave basis set, Comput. Mater. Sci. 6 (1996) 15–50.
[16] G. Kresse, J. Furthmüller, Efficient iterative schemes for ab initio total-energy calculations using a plane-wave basis set, Phys. Rev. B 54 (1996) 11169.
[17] P.E. Blöchl, Projector augmented-wave method, Phys. Rev. B 50 (1994) 17953.
[18] G. Kresse, D. Joubert, From ultrasoft pseudopotentials to the projector augmented-wave method, Phys. Rev. B 59 (1999) 1758.
[19] J.P. Perdew, K. Burke, M. Ernzerhof, Generalized gradient approximation made simple, Phys. Rev. Lett. 77 (1996) 3865.
[20] J.P. Perdew, K. Burke, M. Ernzerhof, Erratum: generalized gradient approximation made simple, Phys. Rev. Lett. 78 (1997) 1396.
[21] M. Methfessel, A. Paxton, High-precision sampling for brillouin-zone integration in metals, Phys. Rev. B 40 (1989) 3616.
[22] C. Wolverton, Solute–vacancy binding in aluminum, Acta Mater 55 (2007) 5867–5872.
[23] S. Plimpton, Fast parallel algorithms for short-range molecular dynamics, J. Comput. Phys. 117 (1995) 1–19.
[24] 2014. http://lammps.sandia.gov.
[25] J.Q. Broughton, F.F. Abraham, N. Bernstein, E. Kaxiras, Concurrent coupling of length scales: methodology and application, Phys. Rev. B 60 (1999) 2391.
[26] N. Govind, Y. Wang, A. Da Silva, E. Carter, Accurate ab initio energetics of extended systems via explicit correlation embedded in a density functional environment, Chem. Phys. Lett. 295 (1998) 129–134.
[27] S. Dapprich, I. Komáromi, K.S. Byun, K. Morokuma, M.J. Frisch, A new oniom implementation in gaussian98. part i. the calculation of energies, gradients, vibrational frequencies and electric field derivatives, Comp. Theor. Chem. 461 (1999) 1–21.
[28] T. Vreven, K. Morokuma, Ö. Farkas, H.B. Schlegel, M.J. Frisch, Geometry optimization with qm/mm, oniom, and other combined methods. i. micro-iterations and constraints, J. Comput. Chem. 24 (2003) 760–769.
[29] T. Vreven, K.S. Byun, I. Komáromi, S. Dapprich, J.A. Montgomery, K. Morokuma, M.J. Frisch, Combining quantum mechanics methods with molecular mechanics methods in oniom, J. Chem. Theory Comput. 2 (2006) 815–826.
[30] T. Junge, G. Anciaux, J.-F. Molinari, Dynamic stability of displacement-based atomistic/continuum coupling methods, J. Mech. Phys. Solids 80 (2015) 103–120.
[31] B.-J. Lee, S.-H. Choi, Computation of grain boundary energies, Model. Simul. Mater. Sci. Eng. 12 (2004) 621.
[32] R. Hadian, Private Correspondence, 2017.
[33] A. Stukowski, Visualization and analysis of atomistic simulation data with ovitothe open visualization tool, Model. Simul. Mater. Sci. Eng. 18 (2010) 015012.
[34] D. Faken, H. Jónsson, Systematic analysis of local atomic structure combined with 3d computer graphics, Comput. Mater. Sci. 2 (1994) 279–286.
[35] H. Tsuzuki, P.S. Branicio, J.P. Rino, Structural characterization of deformed crystals by analysis of common atomic neighborhood, Comput. Phys. Commun. 177 (2007) 518–523.
[36] C.H. Rycroft, G.S. Grest, J.W. Landry, M.Z. Bazant, Analysis of granular flow in a pebble-bed nuclear reactor, Phys. Rev. E 74 (2006) 021306.
[37] D. McLean, Grain Boundary Segregation in Metals, Oxford University Press, 1957.
[38] L. Huber, J. Rottler, M. Militzer, Atomistic simulations of the interaction of alloying elements with grain boundaries in mg, Acta Mater 80 (2014) 194–204.
[39] X. Liu, X. Wang, J. Wang, H. Zhang, First-principles investigation of mg segregation at σ= 11(113) grain boundaries in al, J. Phys. Condens. Matter 17 (2005) 4301.
[40] M. Seah, Adsorption-induced interface decohesion, Acta Metall. 28 (1980) 955–962.
[41] L.-F. Huang, B. Grabowski, E. McEniry, D.R. Trinkle, J. Neugebauer, Importance of coordination number and bond length in titanium revealed by electronic structure investigations, Phys. Status Solidi B 252 (2015) 1907–1924.